Comparison of aerosol optical properties above clouds between POLDER and AeroCom models over the South East Atlantic Ocean during the fire season

Article

Published Version

AGU PUBLICATIONS

Geophysical Research Letters

RESEARCH LETTER
10.1002/2016GL068222

Key Points:
- Above-cloud AOT and SSA retrieved by POLDER are compared with AeroCom models over the South East Atlantic Ocean
- Most models do not reproduce the observed large aerosol load above clouds
- The black carbon refractive index is a key parameter to reproduce POLDER's above-cloud SSA

Correspondence to:
F. Peers,
f.peers@exeter.ac.uk

Citation:
Peers, F., et al. (2016), Comparison of aerosol optical properties above clouds between POLDER and AeroCom models over the South East Atlantic Ocean during the fire season, *Geophys. Res. Lett.*, *43*, doi:10.1002/2016GL068222.

Received 9 SEP 2015
Accepted 5 APR 2016
Accepted article online 7 APR 2016

Comparison of aerosol optical properties above clouds between POLDER and AeroCom models over the South East Atlantic Ocean during the fire season

F. Peers[1,2], N. Bellouin[3], F. Waquet[1], F. Ducos[1], P. Goloub[1], J. Mollard[3], G. Myhre[4], R. B. Skeie[4], T. Takemura[5], D. Tanré[1], F. Thieuleux[1], and K. Zhang[6,7]

[1]Laboratoire d'Optique Atmosphérique, Université Lille 1, Villeneuve d'Ascq, France, [2]Now at College of Engineering, Mathematics, and Physical Sciences, University of Exeter, Exeter, UK, [3]Department of Meteorology, University of Reading, Reading, UK, [4]Center for International Climate and Environmental Research – Oslo, Oslo, Norway, [5]Research Institute for Applied Mechanics, Kyushu University, Fukuoka, Japan, [6]Max Planck Institute for Meteorology, Hamburg, Germany, [7]Pacific Northwest National Laboratory, Richland, Washington, USA

Abstract Aerosol properties above clouds have been retrieved over the South East Atlantic Ocean during the fire season 2006 using satellite observations from POLDER (Polarization and Directionality of Earth Reflectances). From June to October, POLDER has observed a mean Above-Cloud Aerosol Optical Thickness (ACAOT) of 0.28 and a mean Above-Clouds Single Scattering Albedo (ACSSA) of 0.87 at 550 nm. These results have been used to evaluate the simulation of aerosols above clouds in five Aerosol Comparisons between Observations and Models (Goddard Chemistry Aerosol Radiation and Transport (GOCART), Hadley Centre Global Environmental Model 3 (HadGEM3), European Centre Hamburg Model 5-Hamburg Aerosol Module 2 (ECHAM5-HAM2), Oslo-Chemical Transport Model 2 (OsloCTM2), and Spectral Radiation-Transport Model for Aerosol Species (SPRINTARS)). Most models do not reproduce the observed large aerosol load episodes. The comparison highlights the importance of the injection height and the vertical transport parameterizations to simulate the large ACAOT observed by POLDER. Furthermore, POLDER ACSSA is best reproduced by models with a high imaginary part of black carbon refractive index, in accordance with recent recommendations.

1. Introduction

The large uncertainties related to aerosol radiative impacts are a major concern in climate research [*Boucher et al.*, 2013; *Myhre et al.*, 2013a]. When aerosols are horizontally collocated with clouds, the estimation of their radiative forcing is challenging because of the variety and the complexity of the interaction processes. Aerosols have a direct impact on the Earth radiative budget by scattering and absorbing radiations. These interactions influence the vertical profile of temperature and humidity, which affects the formation and the development of clouds (semidirect effect). Aerosols have also an impact on the cloud albedo, lifetime, and precipitation by acting as cloud condensation nuclei (indirect effects). Therefore, overlapping of aerosol and cloud layers is a key situation that helps understand the aerosol impacts on the Earth system.

The South East Atlantic Ocean (SEAO) is a particularly good region for analyzing the full range of aerosol perturbations [*Keil and Haywood*, 2003]. From June to September, biomass burning aerosols are injected into the atmosphere in Southern Africa and are often transported westward to the coast. Smoke plumes are frequently observed above the semipermanent deck of stratocumulus clouds over the ocean [*Devasthale and Thomas*, 2011]. Composed of a complex combination of black and organic carbon [*Saleh et al.*, 2014], smoke aerosol plumes absorb UV and visible light. Above highly reflective clouds, their Direct Radiative Effect (DRE) is usually positive because aerosol absorption reduces local planetary albedo. Recent studies based on remote sensing observations have shown that the DRE of Above-Cloud Aerosols (ACA) is typically strong over the SEAO and can reach instantaneous values larger than +130 Wm^{-2} [*DeGraaf et al.*, 2012; *Peers et al.*, 2015]. However, global aerosol models do not reproduce such high DRE [*DeGraaf et al.*, 2014]. Moreover, a large spread in DRE estimates is observed within AeroCom (Aerosol Comparisons between Observations and Models) models in this region [*Myhre et al.*, 2013b; *Stier et al.*, 2013]. This highlights the need to better constrain aerosol and cloud properties, and especially those controlling the DRE of ACA: the amount of aerosols above clouds, their absorption, and the albedo of the underlying clouds. In this study, the first two parameters will be addressed.

In the last few years, methods have been developed to derive aerosol properties above clouds from passive satellite measurements. On the one hand, Ozone Monitoring Instrument (OMI) and Moderate Resolution Imaging Spectroradiometer (MODIS) observations have been used to retrieve simultaneously the Above-Cloud Aerosol Optical Thickness (ACAOT) and cloud properties, such as the Aerosol-Corrected Cloud Optical Thickness (ACCOT) and the cloud droplet effective radius [*Torres et al.*, 2012; *Jethva et al.*, 2013; *Meyer et al.*, 2015]. However, those algorithms rely on a prescription of an aerosol model, notably their Above-Cloud Single Scattering Albedo (ACSSA), because total radiances are mostly sensitive to the absorption of the overlaying aerosols. On the other hand, polarized radiances provide and additional constraint because they carry the scattering of the aerosol layer above liquid clouds [*Waquet et al.*, 2009]. POLDER (Polarization and Directionality of Earth Reflectances) aboard the PARASOL (Polarization and Anisotropy of Reflectances for Atmospheric Science coupled with Observations from a Lidar) satellite [*Tanré et al.*, 2011] has the unique capability of measuring not only total radiances but also polarized radiances for several wavelengths and viewing angles. In order to fully exploit the potential of this instrument, the method developed by *Waquet et al.* [2013a, 2013b] to retrieve the ACAOT from polarized measurement has been recently improved with total radiances [*Peers et al.*, 2015] and now also retrieves the ACSSA and the ACCOT. Those new remote sensing retrievals offer new possibilities to assess more aspects of the numerical simulations of aerosols. *DeGraaf et al.* [2014] have carried out a comparison of the aerosol DRE obtained with Scanning Imaging Absorption Spectrometer for Atmospheric Chartography with the HadGEM2 model. However, comparing aerosol properties (i.e., ACAOT and ACSSA) is necessary to understand the processes responsible for diversity in modeled DREs.

This study aims at illustrating the potential of the new POLDER products to constrain the aerosol properties simulated by five global models that participated in AeroCom phase II [*Myhre et al.*, 2013b]. The POLDER algorithm has been applied to the SEAO region during the fire season. Descriptions of the POLDER retrieval, the analyzed models, and the comparison methodology are given in section 2. Results are presented in section 3, and explanations of the observed differences between models and POLDER are discussed in section 4. Finally, section 5 summarizes the main findings.

2. Data and Method

2.1. POLDER Aerosol-Above-Cloud Properties

The multidirectional polarized and total radiances measured by POLDER are used in a complementary way. The first step of the aerosol retrieval consists in the estimation of the scattering AOT and aerosol size distribution. The polarized signal of liquid clouds is characterized by a large peak at a scattering angle $\Theta \approx 140°$, which is called the cloud bow, and a small amount of polarization at side scattering angles (i.e., $\Theta < 130°$). Because the polarized signature only comes from the upper cloud layer, it no longer depends on the COT when the COT is larger than 3 [*Goloub et al.*, 1994]. When aerosols are located above clouds, the extinction leads to a reduction of the cloud bow, while scattering processes from the fine mode generates an additional polarization at side scattering angles. Consequently, the scattering AOT and the fine-mode aerosol effective radius are retrieved based on the signal acquired for $\Theta < 130°$ at 670 and 865 nm. The second step of the algorithm is dedicated to the simultaneous retrieval of the Above-Cloud Absorption AOT (ACAAOT) and the COT with total radiances. While the signal produced at the top of the clouds is almost spectrally neutral from UV to shortwave infrared wavelengths [*DeGraaf et al.*, 2012], the spectral signature of the aerosol absorption leads to a stronger impact on radiances at shorter wavelengths. This is called the color-ratio effect [*Jethva et al.*, 2013]. Once scattering AOT and aerosol size are known, radiances at 490 nm and 865 nm can be interpreted as a pair of COT and ACAAOT. Both parts of the retrieval are based on a look-up table approach. The retrieval is attempted for each $6 \times 6\ km^2$ POLDER pixel with $COT \geq 3$. To enhance the quality of the product, several filters are applied. Notably, inhomogeneous clouds are rejected, which represents less than 17% of the observations over the SEAO in August and September 2006. More details about the algorithm and the applied filters are provided in the papers of *Waquet et al.* [2013a, 2013b] and *Peers et al.* [2015]. The POLDER Level 1 products used in this analysis correspond to the PARASOL Collection 2 v03.02.

The accuracy of the retrieved aerosol properties mainly depends on the assumption made about the real part of the refractive index (1.47) and the approximation that polarized radiances only account for the scattering AOT. The impacts of both assumptions on the retrieval have been assessed in Figure 5 of *Peers et al.* [2015]. In this analysis, the uncertainty on the ACAOT and the ACSSA has been evaluated for each inversion by

Table 1. Model General Description[a]

Model	Type	Resolution	Levels	Meteorology	Aerosol Injection Over the Southern Africa	BC and OC Lifetime (days)	BC Refractive Index	Responsible	References
GOCART-v4	CTM	2.5° × 2.0°	30	GEOS-4 DAS (Goddard Earth Observing System version 4 Data Assimilation System), reanalysis for year 2006	Biomass emission in the boundary layer	BC: 6.1OC: 5.0	1.75–0.44i	Thomas DiehlMian Chin	*Chin et al.* [2000, 2002, 2009]; *Ginoux et al.* [2001]
HadGEM3-A	GCM	1.8° × 1.2°	85	ERA Interim data for 2008, nudged	Biomass emission in the boundary layer	BC: 4.1OC: 4.0	1.85–0.71i	Nicolas BellouinJames Mollard	*Bellouin et al.* [2011, 2013]
ECHAM5-HAM2	GCM	1.8° × 1.8°	31	Model nudged with European Centre for Medium-Range Weather Forecasts (ECMWF) analysis for the year 2006	Maximum emission height around 2 km over [*Dentener et al.*, 2006]	BC: 5.9POA: 6.4	1.85–0.71i	Ulrike LohmannPhilip StierKai Zhang	*Vignati et al.* [2004]; *Stier et al.* [2005]; *Zhang et al.* [2012]
OsloCTM2-v2	CTM	2.8° × 2.8°	60	ECMWF reanalysis from the Integrated Forecast System model for year 2006	Emission injection height from project RETRO [*Schultz et al.*, 2007], between 0 and 5 km	BC: 6.3OM: 5.1	variable and mixture with OC	Gunnar MyhreRagnhild B. SkeieTerje Berntsen	*Myhre et al.* [2007, 2009]; *Skeie et al.* [2011]
SPRINTARS-v384	GCM	1.1° × 1.1°	56	National Centers for Environmental Prediction /National Center for Atmospheric Research reanalysis (temperature and horizontal wind), nudged (year 2006)	Emission of carbonaceous aerosol from biomass burning below around 3 km [*Takemura et al.*, 2000]	BCPOM: 5.9	1.75–0.44i	Toshihiko Takemura	*Takemura et al.* [2005, 2009]

[a]CTM: Chemistry Transport Model, GCM: general circulation model, BC: black carbon, OC: organic carbon, POA: primary organic aerosol, OM: organic matter, BCPOM: black carbon and particulate organic matter.

reporting these errors. Additionally, the cloud top height (CTH) has been estimated with POLDER based on the apparent O_2 pressure method [*Vanbauce et al.*, 2003] since the presence of an aerosol layer above clouds has little impact on the retrieval [*Waquet et al.*, 2009].

2.2. AeroCom Models and Comparison Methodology

The AeroCom project brings together international global aerosol models in order to better understand and reduce model diversity by using common experimental data protocols and emission inventories. Five models have supplied the daily profiles needed for this analysis: Goddard Chemistry Aerosol Radiation and Transport (GOCART), Hadley Centre Global Environmental Model 3 (HadGEM3), European Centre Hamburg Model 5-Hamburg Aerosol Module 2 (ECHAM5-HAM2), Oslo-Chemical Transport Model 2 (OsloCTM2), and Spectral Radiation-Transport Model for Aerosol Species (SPRINTARS). The runs correspond to the AeroCom control simulations (A2-CTRL-06) [*Schulz et al.*, 2009]. Model descriptions are given in Table 1, and additional information can be found in *Myhre et al.* [2013b].

In order to select aerosols above clouds only, we have used daily vertical profiles of the aerosol extinction, the aerosol absorption, and the cloud fraction (CF). In absence of more detailed information about clouds (e.g., the liquid water content), CF profiles have been used to identify the location of the modeled cloud layer. The CTH is defined as the altitude where the CF becomes larger than 15% assuming maximum overlap. Since the POLDER algorithm rejects the events contaminated by cirrus, the presence of clouds is not taken into account in models for altitude larger than 4 km, where clouds are most likely

in ice or mixed phase. The aerosol extinction and absorption are then integrated from the top of the atmosphere to the cloud top height in order to compute ACAOT and ACAAOT. Finally, each $6 \times 6\,km^2$ POLDER observation is compared with the co-located modeled aerosol properties. For each model, comparison to POLDER is done only where both POLDER and the model have clouds.

The impact of the CF threshold has been examined by considering thresholds of $15\% \pm 3\%$. Because the modeled vertical profile of CF shows a well-defined layer at low altitude, the threshold has a small impact, with a maximum mean change of ±3% only for the ACAOT and less than ±1% for the ACSSA.

3. Results

The comparison between POLDER and AeroCom models is performed in terms of CTH, ACAOT, and ACSSA at 550 nm over the SEAO region (5°N–30°S, 20°E–20°W) for the fire season 2006. Figure 1 shows the ACAOT and ACSSA time series from June to October. Variation of the POLDER ACAOT is consistent with the DRE seasonality observed by *DeGraaf et al.* [2014]. On average over the 5 months, POLDER retrieves an ACAOT equal to 0.28 with an uncertainty interval ranging from 0.26 to 0.36. The ACAOT derived from models shows a large spread. OsloCTM2 is the model that best reproduces the satellite estimations of the ACAOT regarding both the temporal evolution (e.g., the peaks in July, August, and September) and the average over the period (i.e., 0.26). The ACAOT derived from GOCART is half that of POLDER with a mean value of 0.15. The amount of aerosols above clouds in HadGEM3, ECHAM5-HAM2, and SPRINTARS hardly exceeds 0.1 with averages of 0.08, 0.09, and 0.09, respectively. The analysis of the mean SSA profiles for August–September have revealed a distinct above-cloud layer in all models. This indicates that no significant amount of biomass burning aerosols is located within the cloud. The temporal evolution of the aerosol absorption from POLDER can be divided in two periods. The ACSSA decreases from 0.89 in June to a minimum of 0.84 at the beginning of July. Then, a steady upward trend is observed reaching ACSSA = 0.92 in late October. From June to October, POLDER has retrieved a mean ACSSA of 0.87 ± 0.02. All five models reproduce the temporal evolution of the ACSSA, which is most likely due to the seasonal variation of biomass burning black carbon emissions. Simulations of ACSSA can be split into two groups. First, OsloCTM2 and SPRINSTARS give higher ACSSA estimations with mean values of 0.90 and 0.94. Second, the ACSSA derived from GOCART, HadGEM3, and ECHAM5-HAM2 are closer to POLDER with averages of 0.87, 0.87, and 0.86, respectively. However, no model reproduces the small ACSSA retrieved at the beginning of June. Note that it can be more difficult to retrieve the aerosol size distribution from polarized measurements for small aerosol load, which can impact the ACSSA estimation. In June, the extinction Ångström exponent is around 1.9 in this region, which is consistent with biomass burning particles. The low POLDER ACSSA could also be explained by the increased burning activity in Namibia due to the early-dry season burn policy introduced there in 2006 [*Pricope and Binford*, 2012].

We now focus on August and September, when the aerosol load above clouds is largest. Figure 2 shows the POLDER and the modeled ACAOT and ACSSA. POLDER retrieves the largest ACAOT next to the coast for latitudes between 0°S and 10°S. Averaged ACSSA lower than 0.86 are observed between 10°S and 20°S close to the aerosol source and the ACSSA increases as the smoke outflow gets further from the coast. All models are able to represent the transport of aerosols to the ocean. This is partly because models nudged their meteorology to reanalyses. The spatial distribution of the ACSSA is better reproduced by HadGEM3 and OsloCTM2 than GOCART, which obtains the lowest ACSSA at latitudes under 20°S, associated with the lowest ACAOT.

Figure 3 shows the probability density function (PDF) of the CTH, the ACAOT and the ACSSA, respectively. The distribution of the POLDER CTH peaks at 1.1 km (Figure 3a), which is consistent with previous CALIOP observations in this region [*Chand et al.*, 2009]. The GOCART, HadGEM3, and OsloCTM2 CTH are close to the POLDER estimations. The ECHAM5-HAM2 and the SPRINTARS PDF peaks at lower altitudes (i.e., around 0.6 km), and the distribution is wider in ECHAM5-HAM2. However, the CTH derived from the models is situated within a reasonably narrow range of values, which validates our detected of cloud layer in the models.

The POLDER ACAOT has a large temporal and spatial variability (Figure 3b), with a standard deviation (SD) of 0.23. It reveals that the presence of aerosols above clouds is due to sporadic particle plumes. Apart from OsloCTM2 that efficiently reproduces the POLDER PDF, the distributions of other models are too narrow and shifted to small ACAOTs. This lack of large aerosol loads above clouds is one reason that prevents these models from giving high instantaneous DRE values [*DeGraaf et al.*, 2014].

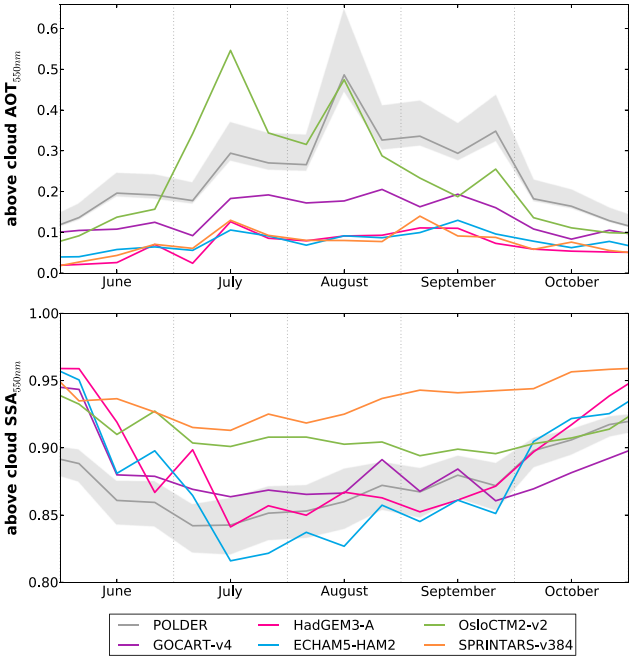

Figure 1. Time series of the ACAOT and ACSSA at 550 nm over the SEAO (5°N–30°S, 20°E–20°W) for the fire season 2006. Each point corresponds to a 10 day average. The gray zone corresponds to the POLDER retrieval uncertainty.

In order to compare the ACSSA of events with the most important potential radiative impact, Figure 3c shows only the ACSSA for 30% of events with the largest ACAOT. The POLDER distribution peaks at 0.87 ± 0.02, which covers both the GOCART and the HadGEM3 mean values (0.88 and 0.85). The peaks of the ECHAM5-HAM2 and the OsloCTM2 distribution are close with averages of 0.84 and 0.90. The aerosols above clouds derived from SPRINTARS are the most scattering with a mean ACSSA of 0.94. The seasonal variations of the ACSSA are larger than retrieval errors with a SD of 0.023 ± 0.004. The spread of the GOCART and HadGEM3 distribution is consistent with POLDER (SD of 0.025 and 0.023). The variability of the ACSSA derived from ECHAM5-HAM2 is twice as large as that of POLDER (SD = 0.046). In contrast, the OsloCTM2 and SPRINTARS distributions are sharp (SD of 0.010 and 0.016). In order to assess the validity of the POLDER comparison, AERONET level 2.0 SSA retrievals for inland sites of Southern Africa (10°S–35°S, 10°E–40°E) in August and September have been co-located with SSAs from models. The data set stretches from 1995 to 2014, which represents 483 successful retrievals. Figure 3d displays the PDF obtained for clear-sky SSA. The distribution for ECHAM5-HAM2 is not shown because data were not available. The AERONET distribution peaks at a slightly lower SSA (0.85) than POLDER. In the same way, the modeled absorption is stronger in Figure 3d than in Figure 3c. Those differences may be due to aging processes during the aerosol transport from land to ocean [*Sayer et al.*, 2014]. Also, clear-sky SSA characterizes the entire atmospheric column, unlike ACSSA which isolates the aerosol layer transported aloft. Otherwise, POLDER brings a similar constraint to AERONET, but with a much improved spatial coverage and much more observations. In summary, OsloCTM2 and SPRINTARS overestimate the SSA, while GOCART and HadGEM3 are closer to POLDER retrievals.

4. Discussion

The differences between the modeled ACAOT and ACSSA partly explain the large spread of the aerosol radiative impact over the SEAO [*Myhre et al.*, 2013b]. This comparison suggests that AeroCom models underestimate the aerosol DRE above clouds because they underestimate the amount of aerosols and/or overestimate the ACSSA. Diversity in modeled cloud albedo would also contribute, but the model distributions required are not available in AeroCom. The reasons of the diversity in the modeled aerosol optical properties above clouds are investigated further below.

First, the diversity in the modeled ACAOT can result from differences in the aerosol removal processes and transport or in the injection of emissions. Lifetimes of organic carbon and black carbon (BC) aerosols are given in Table 1. There is no correlation between aerosol lifetimes and ACAOT. Therefore, the underestimation of the ACAOT does not seem to come from too strong removal processes. However, global lifetimes are probably not representative of aerosols in the SEAO region. Additionally, we have analyzed the importance of the vertical aerosol profile. The aerosol vertical distribution has been qualitatively assessed near biomass burning sources (20°N–20°S, 20°E–30°E) by calculating the mean extinction height Z_α [*Koffi et al.*, 2012]. In August to September, OsloCTM2 has a Z_α of 2.08 km, which is comparable to the 2.03 km observed by CALIOP over

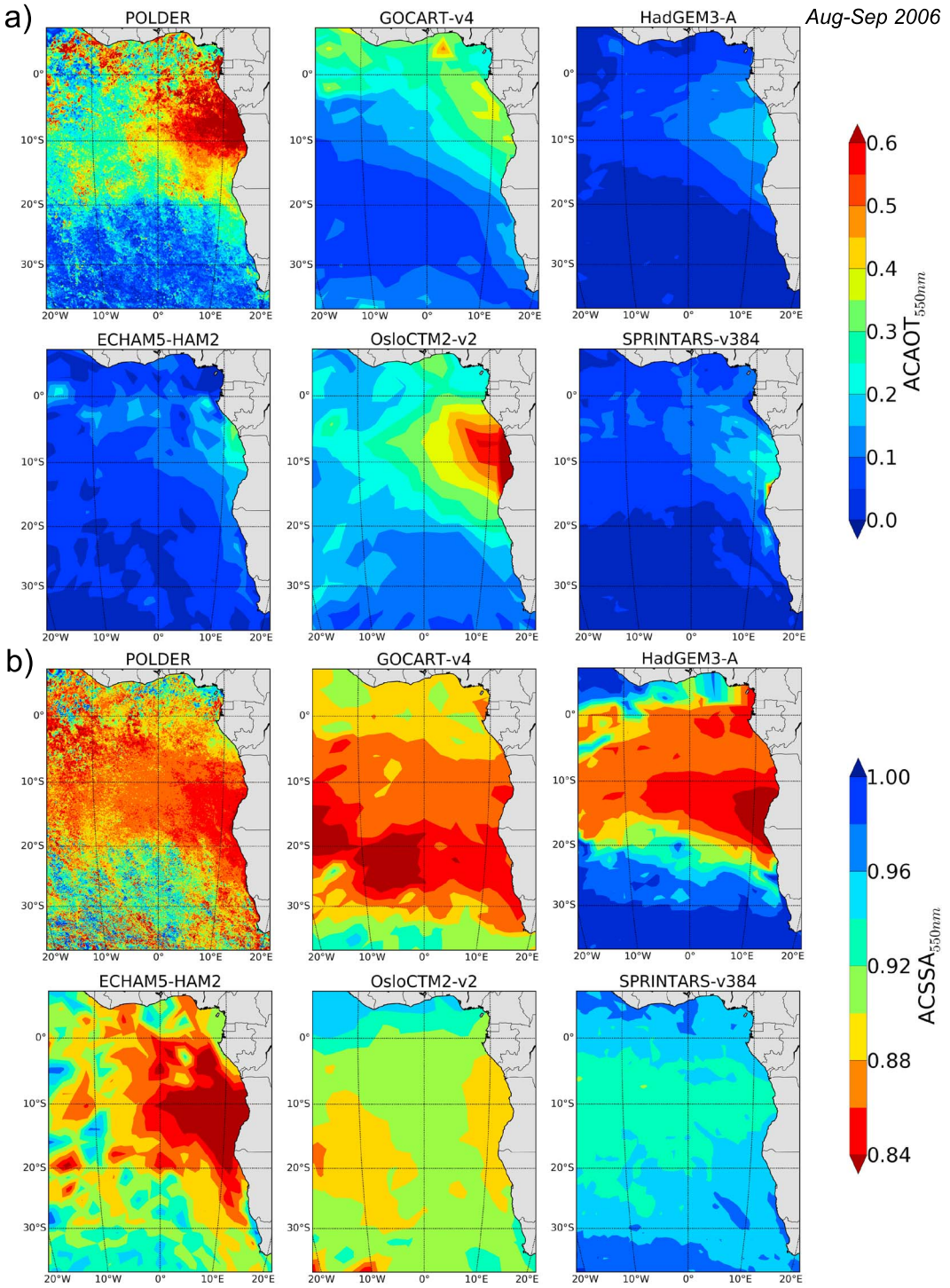

Figure 2. (a) ACAOT and (b) ACSSA at 550 nm over the SEAO from August to September 2006.

approximately the same area (20°N–20°S, 0°E–45°E) in September–November [*Koffi et al.*, 2012]. For the other models, aerosols are located at lower altitudes: Z_α is 1.44, 1.30, 1.33, and 1.22 km for GOCART, HadGEM3, ECHAM5-HAM2, and SPRINTARS, respectively. Consequently, a correct Z_α is important to simulate a realistic distribution of ACAOT. A reason for the larger Z_α of OsloCTM2 could be its higher injection height: it is the only model to emit aerosols above the boundary layer in Southern Africa. However, the model-based analysis of *Veira et al.* [2015a] has shown that only a small fraction of plumes reaches the free troposphere. Also, most

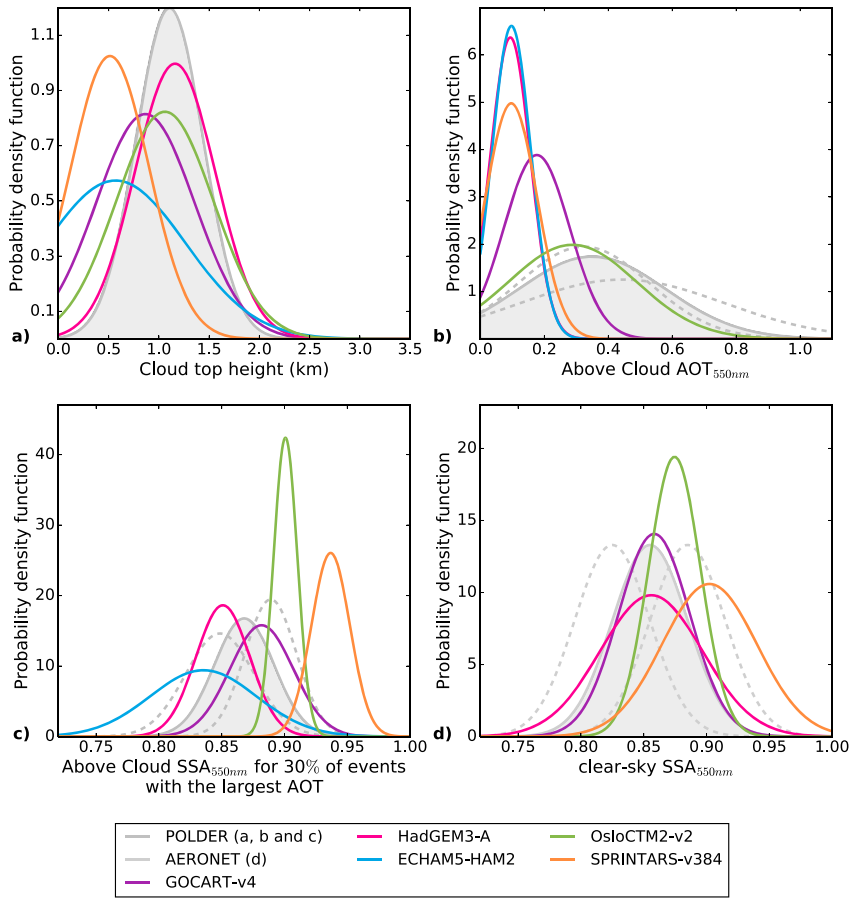

Figure 3. (a–c) Probability density function (PDF) of aerosol and cloud properties in ACA scenes over the SEAO (5°N–30°S, 20°E–20°W) for August to September 2006. Dashed gray lines correspond to the boundaries of the POLDER retrieval uncertainty for the ACAOT and the ACSSA. (d) PDF of clear-sky SSA. AERONET level 2 retrievals are compared with co-located SSA derived from AeroCom models for August to September 1995–2014 over Southern Africa (10°N–35°S, 40°E–10°W). Dashed gray lines correspond to the boundaries of the AERONET retrieval uncertainty for the SSA. (List of AERONET sites: Bethlehem, Durban UKZN, Elandsfontein, Etosha Pan, Gorongosa, Inhaca, Joberg, Kaloma, Maun Tower, Mfuwe, Mongu, Mongu Inn, Mwinilunga, Ndola, Pietersburg, Pretoria CSIR-DPSS, Senanga, Sesheke, Skukuza, SKUKUZA AEROPORT, Solwezi, Wits University, and Zambezi).

of the source are located at altitudes higher than the marine boundary layer. In the absence of vertical transport, this implies that smoke is already injected at altitudes higher than the clouds. Consequently, differences in emission heights do not fully explain differences in modeled aerosol vertical profiles [*Kipling et al.*, 2013; *Veira et al.*, 2015b]. The strength of the vertical transport, which depends on the convection parameterization in models, also controls the aerosol vertical distribution, suggesting that model calibration is necessary.

Second, our study reveals the large diversity in the modeled ACSSA. ECHAM5-HAM2 and HadGEM3 are the models that better reproduce both the spatial distribution and mean of the ACSSA. Both models prescribe a high imaginary part of the BC refractive index (0.71) following the recommendation of *Bond and Bergstrom* [2006]. In contrast, the BC prescription of GOCART and SPRINTARS is less absorbing with an imaginary part of the refractive index of 0.44, based on the *WCP* model [1986]. OsloCTM2 has combined properties for BC and organic aerosols (OA) and its SSA for aged biomass burning aerosols is 0.91 at low relative humidity. The mass ratio of BC to OA also affects the SSA. Column-integrated BC:OA ratio for August–September over the SEAO is similar for HadGEM3, OsloCTM2, and SPRINTARS (5.4%, 6.2%, and 6.1%, respectively), confirming that differences in the modeled ACSSA come from the prescription of the BC refractive index. To quantify the impact of the BC:OC ratio, Mie calculations of the SSA have been performed, assuming a single mode lognormal number size distribution with a geometric mean radius of 0.12 μm and a standard deviation of 1.30, which is consistent with the measurements performed during the SAFARI 2000 campaign for aged

biomass burning aerosols [*Haywood et al.*, 2003]. For a BC:OA ratio of 5.5%, the SSA is 0.91 when the WCP refractive index of BC is used, as in SPRINTARS, but decreases to 0.86 with the more recent BC prescription, as in HadGEM3. ECHAM5-HAM2 and GOCART have a higher BC:OA ratio (11.8% and 7.8%). For a ratio of 7.5%, the SSA obtained with the less absorbing BC prescription is 0.88. It decreases to 0.82 when the more absorbing BC refractive index is considered. Therefore, using a recent BC prescription allows reproducing the low SSA observed by POLDER. In addition, the low ACSSA modeled by GOCART for small ACAOT are attributed to the large contribution of BC to the aerosol load. At latitude lower than 20°S, the BC:OA ratio is around 8.7%. It could be caused by an over-efficient BC vertical dispersion for GOCART and an underestimation of removal processes [*Schwarz et al.*, 2010, 2013]. The ACSSA of ECHAM5-HAM2 is larger than expected from its large BC:OA ratio because of contributions of third-party species like sea salt or sulfate.

5. Conclusions

Multidirectional polarized and total radiance measurements from POLDER/PARASOL provide sensitivity to the scattering and the absorption of aerosol layers located above liquid clouds. A method has been developed to retrieve the ACAOT and ACSSA and the aerosol-corrected COT when the cloud is homogeneous and optically thick. Retrieved aerosol properties have been compared with AeroCom modeled properties over the SEAO during the fire season 2006. This region is a good test bed for the representation of aerosols in cloudy skies in climate models: the absorbing biomass burning aerosols, frequently observed above clouds, are expected to have an important radiative impact that is currently poorly constrained.

Five AeroCom models have been compared to POLDER, using vertical profiles of the aerosol extinction, the aerosol absorption, and the CF. This analysis demonstrates that the properties of aerosols above clouds are associated with a large variability in the models. The ACAOT is underestimated by four of them, which is likely due to the vertical transport calibration and lower aerosol emission altitudes. This issue is currently analyzed through the Biomass Burning Emissions Experiments of the AeroCom Phase III. The comparison also reveals that models with more absorbing BC tend to better reproduce the low ACSSA observed by POLDER. By either underestimating the aerosol load or the aerosol absorption, all five models underestimate the ACAAOT, suggesting an underestimation of the aerosol DRE over the SEAO. This study demonstrates the usefulness of POLDER retrievals in constraining key aerosol parameters in global aerosol models. The comparison notably highlights the importance of injection heights, vertical transport, and BC refractive index prescription in reproducing the aerosol optical properties above clouds over the SEAO.

The aerosol properties are not the only parameter that determines the aerosol DRE above clouds. The accurate knowledge of the cloud albedo is also important. When additional information about the cloud vertical profile is provided by the models (e.g., the liquid and the frozen water content and the COT), a comparison with POLDER will become possible since the ACA method allows the retrieval of the aerosol-corrected COT as well.

Finally, a global comparison of aerosol properties above clouds would increase the understanding of the factors responsible for model variability. However, the reliability of the method used to select aerosols above clouds in models has only been tested over the SEAO, where the stratocumulus layer is well defined. The use of the CF vertical profile to define the cloud layer becomes difficult for complex cloud covers such as mixed phase clouds or heterogeneous clouds. Once again, additional cloud information is necessary to perform such an analysis.

Acknowledgments

The Chemical and Physical Properties of the Atmosphere project is funded by the French National Research Agency (ANR) through the Programme d'Investissement d'Avenir under contract ANR-11-LABX-0005-01 and by the Regional Council Nord-Pas de Calais and the European Funds for Regional Economic Development. This work was supported by the Programme National de Télédétection Spatiale (PNTS, http://www.insu.cnrs.fr/ pnts), grant PNTS-2013-10. The authors are grateful to the CNES, NASA, and the ICARE data and services center. The Pacific Northwest National Laboratory is operated for DOE by Battelle Memorial Institute under contract DE-AC06-76RLO 1830. Authors are grateful to the Editor and the anonymous reviewer whose insightful comments helped improve the manuscript. The AeroCom database can be accessed by following the instructions on http://aerocom.met.no/data.html. POLDER products are available through the ICARE data and service center (http://www.icare.univ-lille1.fr/) and, for the data set used in this analysis, upon request to Fanny Peers (f.peers@exeter.ac.uk) or Fabien Waquet (fabien.waquet@univ-lille1.fr). The AERONET data are accessible via the web interface http://aeronet.gsfc.nasa.gov/.

References

Bellouin, N., J. Rae, A. Jones, C. Johnson, J. Haywood, and O. Boucher (2011), Aerosol forcing in the Climate Model Intercomparison Project (CMIP5) simulations by HadGEM2-ES and the role of ammonium nitrate, *J. Geophys. Res.*, *116*, D20206, doi:10.1029/2011JD016074.

Bellouin, N., G. W. Mann, M. T. Woodhouse, C. Johnson, K. S. Carslaw, and M. Dalvi (2013), Impact of the modal aerosol scheme GLOMAP-mode on aerosol forcing in the Hadley Centre Global Environmental Model, *Atmos. Chem. Phys.*, *13*(6), 3027–3044.

Bond, T. C., and R. W. Bergstrom (2006), Light absorption by carbonaceous particles: An investigative review, *Aerosol Sci. Technol.*, *40*(1), 27–67.

Boucher, O., et al. (2013), Clouds and aerosols, in *Climate Change 2013: The Physical Science Basis. Contribution of Working Group I to the Fifth Assessment Report of the Intergovernmental Panel on Climate Change*, edited by T. F. Stocker et al., Cambridge Univ. Press, Cambridge, U. K., and New York.

Chand, D., R. Wood, T. Anderson, S. Satheesh, and R. Charlson (2009), Satellite-derived direct radiative effect of aerosols dependent on cloud cover, *Nat. Geosci.*, *2*(3), 181–184, doi:10.1038/ngeo437.

Chin, M., R. B. Rood, S. J. Lin, J. F. Muller, and A. M. Thompson (2000), Atmospheric sulfur cycle simulated in the global model GOCART: Model description and global properties, *J. Geophys. Res.*, *105*, 24,671–24,687, doi:10.1029/2000JD900384.

Chin, M., P. Ginoux, S. Kinne, O. Torres, B. N. Holben, B. N. Duncan, R. V. Martin, J. A. Logan, A. Higurashi, and T. Nakajima (2002), Tropospheric aerosol optical thickness from the GOCART model and comparisons with satellite and Sun photometer measurements, *J. Atmos. Sci.*, *59*, 461–483.

Chin, M., T. Diehl, O. Dubovik, T. F. Eck, B. N. Holben, A. Sinyuk, and D. G. Streets (2009), Light absorption by pollution, dust, and biomass burning aerosols: A global model study and evaluation with AERONET measurements, *Ann. Geophys.*, *27*(9), 3439.

DeGraaf, M., L. Tilstra, P. Wang, and P. Stammes (2012), Retrieval of the aerosol direct radiative effect over clouds from spaceborne spectrometry, *J. Geophys. Res.*, *117*, D07207, doi:10.1029/2011JD017160.

DeGraaf, M., N. Bellouin, L. Tilstra, J. Haywood, and P. Stammes (2014), Aerosol direct radiative effect of smoke over clouds over the southeast Atlantic Ocean from 2006 to 2009, *Geophys. Res. Lett.*, *41*, 7723–7730, doi:10.1002/2014GL061103.

Dentener, F., et al. (2006), Emissions of primary aerosol and precursor gases in the years 2000 and 1750 prescribed data-sets for AeroCom, *Atmos. Chem. Phys.*, *6*(12), 4321–4344.

Devasthale, A., and M. A. Thomas (2011), A global survey of aerosol-liquid water cloud overlap based on four years of CALIPSO-CALIOP data, *Atmos. Chem. Phys.*, *11*(3), 1143–1154.

Ginoux, P., M. Chin, I. Tegen, J. M. Prospero, B. Holben, O. Dubovik, and S. J. Lin (2001), Sources and distributions of dust aerosols simulated with the GOCART model, *J. Geophys. Res.*, *106*, 20,255–20,273, doi:10.1029/2000JD000053.

Goloub, P., J. L. Deuzé, M. Herman, and Y. Fouquart (1994), Analysis of the POLDER polarization measurements performed over cloud covers, geoscience and remote sensing, *IEEE Trans.*, *32*(1), 78–88, doi:10.1109/36.285191.

Haywood, J. M., S. R. Osborne, P. N. Francis, A. Keil, P. Formenti, M. O. Andreae, and P. H. Kaye (2003), The mean physical and optical properties of regional haze dominated by biomass burning aerosol measured from the C-130 aircraft during SAFARI 2000, *J. Geophys. Res.*, *108*(D13), 8473, doi:10.1029/2002JD002226.

Jethva, H., O. Torres, L. Remer, and P. Bhartia (2013), A color ratio method for simultaneous retrieval of aerosol and cloud optical thickness of above-cloud absorbing aerosols from passive sensors: Application to MODIS measurements, *IEEE Trans. Geosci. Remote Sens.*, *51*(7), 3862–3870, doi:10.1109/TGRS.2012.2230008.

Keil, A., and Haywood, J. M. (2003), Solar radiative forcing by biomass burning aerosol particles during SAFARI 2000: A case study based on measured aerosol and cloud properties, *J. Geophys. Res.*, *108*(D13), 8467, doi:10.1029/2002JD002315.

Kipling, Z., P. Stier, J. P. Schwarz, A. E. Perring, J. R. Spackman, G. W. Mann, C. E. Johnson, and P. J. Telford (2013), Constraints on aerosol processes in climate models from vertically-resolved aircraft observations of black carbon, *Atmos. Chem. Phys.*, *13*(12), 5969–5986.

Koffi, B., et al. (2012), Application of the CALIOP layer product to evaluate the vertical distribution of aerosols estimated by global models: AeroCom phase I results, *J. Geophys. Res.*, *117*, D10201, doi:10.1029/2011JD016858.

Meyer, K., S. Platnick, and Z. Zhang (2015), Simultaneously inferring above-cloud absorbing aerosol optical thickness and underlying liquid phase cloud optical and microphysical properties using MODIS, *J. Geophys. Res. Atmos.*, *120*, 5524–5547, doi:10.1002/2015JD023128.

Myhre, G., et al. (2007), Comparison of the radiative properties and direct radiative effect of aerosols from a global aerosol model and remote sensing data over ocean, *Tellus B*, *59*(1), 115–129.

Myhre, G., et al. (2009), Modelled radiative forcing of the direct aerosol effect with multi-observation evaluation, *Atmos. Chem. Phys.*, *9*(4), 1365–1392.

Myhre, G., et al. (2013a), Anthropogenic and Natural Radiative Forcing, in *Climate Change 2013: The Physical Science Basis. Contribution of Working Group I to the Fifth Assessment Report of the Intergovernmental Panel on Climate Change*, edited by T. F. Stocker et al., Cambridge Univ. Press, Cambridge, U. K., and New York.

Myhre, G., et al. (2013b), Radiative forcing of the direct aerosol effect from AeroCom Phase II simulations, *Atmos. Chem. Phys.*, *13*(4), 1853–1877, doi:10.5194/acp-13-1853-2013.

Peers, F., F. Waquet, C. Cornet, P. Dubuisson, F. Ducos, P. Goloub, F. Szczap, D. Tanré, and F. Thieuleux (2015), Absorption of aerosols above clouds from POLDER/PARASOL measurements and estimation of their direct radiative effect, *Atmos. Chem. Phys.*, *15*(8), 4179–4196, doi:10.5194/acp-15-4179-2015.

Pricope, N. G., and M. W. Binford (2012), A spatio-temporal analysis of fire recurrence and extent for semi-arid savanna ecosystems in southern Africa using moderate-resolution satellite imagery, *J. Environ. Manag.*, *100*, 72–85.

Saleh, R., et al. (2014), Brownness of organics in aerosols from biomass burning linked to their black carbon content, *Nat. Geosci.*, doi:10.1038/ngeo2220.

Sayer, A. M., N. C. Hsu, T. F. Eck, A. Smirnov, and B. N. Holben (2014), AERONET-based models of smoke-dominated aerosol near source regions and transported over oceans, and implications for satellite retrievals of aerosol optical depth, *Atmos. Chem. Phys.*, *14*(20), 11,493–11,523.

Schultz, M., M. van het Bolscher, T. Pulles, R. Brand, J. Pereira, and A. Spessa (2007), RETRO report on emission data sets and methodologies for estimating emissions, Workpackage 1, Deliverable D1-6, 2007; EU-Contract No. EVK2-CT-2002-00170.

Schulz, M., M. Chin, and S. Kinne (2009), The aerosol model comparison project, AeroCom, phase II: Clearing up diversity, IGAC Newsletter, (41).

Schwarz, J. P., J. R. Spackman, R. S. Gao, L. A. Watts, P. Stier, M. Schulz, S. M. Davis, S. C. Wofsy, and D. W. Fahey (2010), Global-scale black carbon profiles observed in the remote atmosphere and compared to models, *Geophys. Res. Lett.*, *37*, L18812, doi:10.1029/2010GL044372.

Schwarz, J. P., B. H. Samset, A. E. Perring, J. R. Spackman, R. S. Gao, P. Stier, M. Schulz, F. L. Moore, E. A. Ray, and D. W. Fahey (2013), Global-scale seasonally resolved black carbon vertical profiles over the Pacific, *Geophys. Res. Lett.*, *40*, 5542–5547, doi:10.1002/2013GL057775.

Skeie, R. B., T. Berntsen, G. Myhre, C. A. Pedersen, J. Ström, S. Gerland, and J. A. Ogren (2011), Black carbon in the atmosphere and snow, from pre-industrial times until present, *Atmos. Chem. Phys.*, *11*(14), 6809–6836.

Stier, P., et al. (2005), The aerosol-climate model ECHAM5-HAM, *Atmos. Chem. Phys.*, *5*, 1125–1156, doi:10.5194/acp-5-1125-2005.

Stier, P., et al. (2013), Host model uncertainties in aerosol radiative forcing estimates: Results from the AeroCom Prescribed intercomparison study, *Atmos. Chem. Phys.*, *13*(6), 3245–3270, doi:10.5194/acp-13-3245-2013.

Takemura, T., H. Okamoto, Y. Maruyama, A. Numaguti, A. Higurashi, and T. Nakajima (2000), Global three-dimensional simulation of aerosol optical thickness distribution of various origins, *J. Geophys. Res.*, *105*(D14), 17,853–17,873, doi:10.1029/2000JD900265.

Takemura, T., T. Nozawa, S. Emori, T. Y. Nakajima, and T. Nakajima (2005), Simulation of climate response to aerosol direct and in- direct effects with aerosol transport-radiation model, *J. Geophys. Res.*, *110*, D02202, doi:10.1029/2004JD005029.

Takemura, T., M. Egashira, K. Matsuzawa, H. Ichijo, R. O'Ishi, and A. Abe-Ouchi (2009), A simulation of the global distribution and radiative forcing of soil dust aerosols at the Last Glacial Maximum, *Atmos. Chem. Phys.*, *9*, 3061–3073, doi:10.5194/acp-9-3061-2009.

Tanré, D., F. Bréon, J. Deuzé, O. Dubovik, F. Ducos, P. François, P. Goloub, M. Herman, A. Lifermann, and F. Waquet (2011), Remote sensing of aerosols by using polarized, directional and spectral measurements within the A-Train: the PARASOL mission, *Atmos. Meas. Tech.*, *4*(7), 1383–1395, doi:10.5194/amt-4-1383-2011.

Torres, O., H. Jethva, and P. Bhartia (2012), Retrieval of aerosol optical depth above clouds from OMI observations: Sensitivity analysis and case studies, *J. Atmos. Sci.*, *69*(3), 1037–1053, doi:10.1175/JAS-D-11-0130.1.

Vanbauce, C., B. Cadet, and R. T. Marchand (2003), Comparison of POLDER apparent and corrected oxygen pressure to ARM/MMCR cloud boundary pressures, *Geophys. Res. Lett.*, *30*(5), 1212, doi:10.1029/2002GL016449.

Veira, A., S. Kloster, S. Wilkenskjeld, and S. Remy (2015a), Fire emission heights in the climate system–Part 1: Global plume height patterns simulated by ECHAM6-HAM2, *Atmos. Chem. Phys. Discuss.*, *15*(5), 6645–6693.

Veira, A., S. Kloster, N. A. J. Schutgens, and J. W. Kaiser (2015b), Fire emission heights in the climate system–Part 2: Impact on transport, black carbon concentrations and radiation, *Atmos. Chem. Phys. Discuss.*, *15*(5), 6695–6744.

Vignati, E., J. Wilson, and P. Stier (2004), M7: An efficient size-resolved aerosol microphysics module for large-scale aerosol transport models, *J. Geophys. Res.*, *109*, D22202, doi:10.1029/2003JD004485.

Waquet, F., J. Riedi, L. Labonnote, P. Goloub, B. Cairns, J.-L. Deuzé, and D. Tanré (2009), Aerosol remote sensing over clouds using A-Train observations, *J. Atmos. Sci.*, *66*(8), 2468–2480, doi:10.1175/2009JAS3026.1.

Waquet, F., et al. (2013a), Retrieval of aerosol microphysical and optical properties above liquid clouds from POLDER/PARASOL polarization measurements, *Atmos. Meas. Tech.*, *6*(4), 991–1016, doi:10.5194/amt-6-991-2013.

Waquet, F., F. Peers, F. Ducos, P. Goloub, S. Platnick, J. Riedi, D. Tanré, and F. Thieuleux (2013b), Global analysis of aerosol properties above clouds, *Geophys. Res. Lett.*, *40*, 5809–5814, doi:10.1002/2013GL057482.

WCP (1986), A preliminary cloudless standard atmosphere.

Zhang, K., et al. (2012), The global aerosol-climate model ECHAM-HAM, version 2: Sensitivity to improvements in process representations, *Atmos. Chem. Phys.*, *12*, 8911–8949, doi:10.5194/acp-12-8911-2012.